Technical University of Denmark

DTU

Hybrid Ytterbium-doped large-mode-area photonic crystal fiber amplifier for long wavelengths.

Petersen, Sidsel Rübner; Alkeskjold, Thomas T.; Poli, Federica; Coscelli, Enrico; Johansen, Mette Marie; Laurila, Marko; Lægsgaard, Jesper; Broeng, Jes

Link back to DTU Orbit

DTU Library
Technical Information Center of Denmark

Hybrid Ytterbium-doped large-mode-area photonic crystal fiber amplifier for long wavelengths

Sidsel R. Petersen,[1,*] Thomas T. Alkeskjold,[2] Federica Poli,[3] Enrico Coscelli,[3] Mette M. Jørgensen,[1] Marko Laurila,[1] Jesper Lægsgaard,[1] and Jes Broeng[2]

[1]DTU Fotonik, Department of Photonics Engineering, Technical University of Denmark, Denmark
[2]NKT Photonics A/S, Blokken 84, 3460 Birkerød, Denmark
[3]Information Engineering Department, University of Parma, Parma, Italy
[*]srpe@fotonik.dtu.dk

Abstract: A large-mode-area Ytterbium-doped photonic crystal fiber amplifier with build-in gain shaping is presented. The fiber cladding consists of a hexagonal lattice of air holes, where three rows are replaced with circular high-index inclusions. Seven missing air holes define the large-mode-area core. Light confinement is achieved by combined index and bandgap guiding, which allows for single-mode operation and gain shaping through distributed spectral filtering of amplified spontaneous emission. The fiber properties are ideal for amplification in the long wavelength regime of the Ytterbium gain spectrum above 1100 nm, and red shifting of the maximum gain to 1130 nm is demonstrated.

References and links

1. A. Shirakawa, C. B. Olausson, H. Maruyama, K. I. Ueda, J. K. Lyngsø, and J. Broeng, "High power ytterbium fiber lasers at extremely long wavelengths by photonic bandgap fiber technology," Opt. Fiber Technol. **16**(6), 449–457 (2010).
2. N. Saito, K. Akagawa, M. Ito, A. Takazawa, Y. Hayano, Y. Saito, M. Ito, H. Takami, M. Iye, and S. Wada, "Sodium D_2 resonance radiation in single-pass sum-frequency generation with actively mode-locked Nd:YAG lasers," Opt. Lett. **32**(14), 1965–1967 (2007).
3. C. Boyer, B. Ellerbroek, M. Gedig, E. Hileman, R. Joycec, and M. Liang, "Update on the TMT laser guide star facility design," Proc. SPIE **7015**, 70152N, 70152N-12 (2008).
4. J. Limpert, F. Röser, S. Klingebiel, T. Schreiber, C. Wirth, T. Peschel, R. Eberhardt, and A. Tünnermann, "The rising power of fiber lasers and amplifiers," IEEE J. Sel. Top. Quantum Electron. **13**(3), 537–545 (2007).
5. A. Cerqueira S, Jr., F. Luan, C. M. B. Cordeiro, A. K. George, and J. C. Knight, "Hybrid photonic crystal fiber," Opt. Express **14**(2), 926–931 (2006).
6. A. Argyros, T. A. Birks, S. G. Leon-Saval, C. M. B. Cordeiro, and P. St J Russell, "Guidance properties of low-contrast photonic bandgap fibres," Opt. Express **13**(7), 2503–2511 (2005).
7. E. Coscelli, F. Poli, S. R. Petersen, T. T. Alkeskjold, A. Cucinotta, S. Selleri, L. Leick, and J. Broeng, "Anti-symmetric hybrid photonic crystal fibers with enhanced filtering and bending properties," SPIE Photonics West 2012, Jan 21–26, San Francisco CA, USA, paper 8237–129 (2012), (to be published).
8. J. W. Nicholson, A. D. Yablon, S. Ramachandran, and S. Ghalmi, "Spatially and spectrally resolved imaging of modal content in large-mode-area fibers," Opt. Express **16**(10), 7233–7243 (2008).
9. S. Wielandy, "Implications of higher-order mode content in large mode area fibers with good beam quality," Opt. Express **15**(23), 15402–15409 (2007).
10. F. Jansen, F. Stutzki, H.-J. Otto, M. Baumgartl, C. Jauregui, J. Limpert, and A. Tünnermann, "The influence of index-depressions in core-pumped Yb-doped large pitch fibers," Opt. Express **18**(26), 26834–26842 (2010).
11. T. T. Alkeskjold, "Large-mode-area ytterbium-doped fiber amplifier with distributed narrow spectral filtering and reduced bend sensitivity," Opt. Express **17**(19), 16394–16405 (2009).
12. A. Cucinotta, F. Poli, S. Selleri, L. Vincetti, and M. Zoboli, "Amplification properties of Er^{3+}-doped photonic crystal fibers," J. Lightwave Technol. **21**(3), 782–788 (2003).
13. F. Poli, A. Cucinotta, and S. Selleri, *Photonic Crystal Fibers: Properties and Applications*, 1st ed. (Springer, 2007).

14. R. Goto, S. D. Jackson, S. Fleming, B. T. Kuhlmey, B. J. Eggleton, and K. Himeno, "Birefringent all-solid hybrid microstructured fiber," Opt. Express **16**(23), 18752–18763 (2008).
15. J. Nilsson, "High-power fiber sources," SPIE Photonics West, Short Course, sc748, (2011).

1. Introduction

High power fiber amplifiers operating in the spectral range 1100 nm – 1200 nm are desired for frequency-doubling to the yellow-orange light regime. This region finds applications within the medical industry, high-resolution spectroscopy, and astronomical observations [1, 2]. Especially the wavelength of 589 nm is of interest for excitation of sodium atoms in the atmosphere to create a so-called laser guide star. This allows for compensation of atmospheric turbulence to increase the performance of ground based optical telescopes [3].

Ytterbium-doped (Yb-doped) fiber amplifiers are interesting candidates for amplification in this spectral range, due to the broad emission spectrum in the range 900-1200 nm. However, to achieve amplification in the long wavelength region of the Yb emission spectrum, the larger gain at shorter wavelengths near 1030 nm must be suppressed to avoid parasitic lasing due to gain build-up from Amplified Spontaneous Emission (ASE).

Reduction of ASE can be achieved in multi-stage amplifiers with discrete filters inserted between each amplification stage, however, it is a delicate balance between insertion loss and gain. Instead, ASE suppression by spectral filtering incorporated in the fiber cladding can have advantages. Distributed Spectral Filtering (DSF) can be realized using the Photonic BandGap (PBG) effect, which provides confinement of the core mode only in restricted spectral regions. By careful design of the cladding structure, the signal wavelength is confined to the core, while spontaneous emission at shorter wavelengths is filtered, and ASE is suppressed. This results in build-in gain shaping, where the Yb gain maximum can be red shifted from 1030 nm to wavelengths above 1100 nm. Gain shaping has already been demonstrated in all-solid PBG fibers, and amplification at 1178 nm with output power of 167 W has been achieved [1].

Nonlinear effects, such as stimulated Raman scattering, stimulated Brillouin scattering, and four-wave mixing, are the limiting factors for power scaling in high power fiber amplifiers [4]. A fiber amplifier design having a Large-Mode-Area (LMA) core can increase the nonlinear threshold, however, special care should be invested to maintain Single-Mode (SM) guidance with an increasing core size.

The challenges of gain shaping and a SM LMA core design must be met simultaneously to realize an efficient high power fiber amplifier in the long wavelength region of the Yb emission spectrum. Furthermore bending resistance is important to create a compact fiber amplifier. In this work, an asymmetric hybrid Photonic Crystal Fiber (PCF) amplifier for wavelengths above 1100 nm is demonstrated. The fiber can be coiled to diameters of ~30 cm without losing confinement of the core mode.
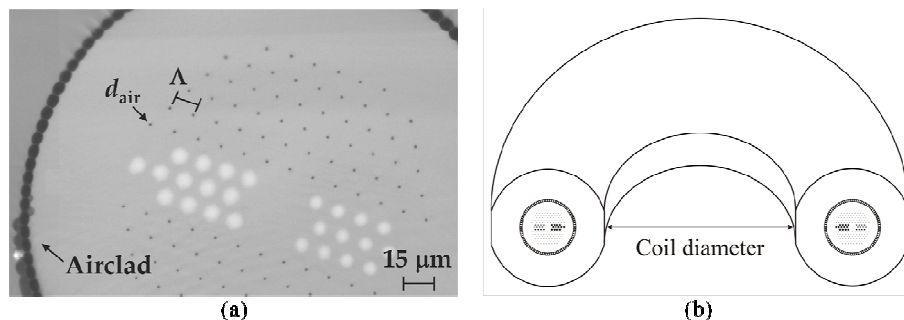

Fig. 1. (a) Microscope image of the asymmetric hybrid large-mode-area photonic crystal fiber. The grey background is silica, the black dots are air holes, and the white regions are Germanium-doped silica. (b) Schematic illustration of the fiber coil control by a double-D-shaped silica jacket.

2. Fiber amplifier design

A microscope image of the considered fiber is shown in Fig. 1(a). The fiber is a double-clad PCF with an airclad as the outer cladding, providing confinement of the pump light. The inner cladding consists of a hexagonal lattice of air holes with diameter d_{air}, and hole-to-hole spacing Λ, Fig. 1(a). Seven missing air holes define the core region. Three rows of air holes on each side of the core are replaced with circular high-index Germanium-doped (Ge-doped) silica rods with NA = 0.29; thereby combining the two guiding mechanisms of PCFs in a hybrid PCF, index and bandgap guiding. Confinement is achieved only when guiding is provided by both mechanisms [5]. The fiber is surrounded by a double-D-shaped silica jacket, which is used for coil control, Fig. 1(b). The flat planes of the double-D-shape ensure the fiber will bend as illustrated.

The diameter of the Ge-doped rods on one side of the core is reduced with respect to the one of those on the other side, resulting in an asymmetric design. The asymmetry introduces an extra degree of freedom in the design possibilities. By tuning the ratio of the large and small Ge-doped rods, both the blue- and red-edge of the transmission windows can be adjusted, as shown in Fig. 2. In Fig. 2(a) the transmission window corresponds to the spectral position of a bandgap caused by the larger Ge-doped rods, while the transmission window in Fig. 2(b) corresponds to a bandgap caused by the small Ge-doped rods. When both sizes are combined in the asymmetric hybrid PCF, confinement is only possible in the spectral regions, where the bandgaps overlap, as shown in Fig. 2(c).

The SM properties of the index guiding PCF combined with gain shaping from the PBG effect of the Ge-doped rods, enables a SM fiber amplifier with a core diameter of ~45 µm working at wavelengths above 1100 nm.
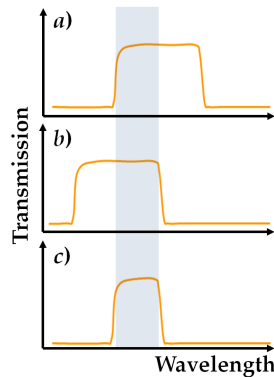

Fig. 2. The guiding properties of the asymmetric hybrid photonic crystal fiber illustrated with transmission spectra. (a) and (b) show transmission windows corresponding to bandgaps caused by the large and small Germanium-doped silica rods, respectively. (c) shows the transmission window of the hybrid photonic crystal fiber where both sizes of Germanium-doped rods are present.

3. Passive fibers

3.1 Bending properties

The bending properties and spectral positions of the transmission bands are investigated for two passive 2 m-long hybrid PCFs, fiber A and fiber B. For fiber A, Λ_A = 10 µm and $d_{air,A}$ = $0.12\Lambda_A$, while for fiber B, Λ_B = 12 µm and $d_{air,B}$ = $0.11\Lambda_B$. The large Ge-doped rods of both PCFs have a diameter of 0.71Λ, while the small Ge-doped rod size is reduced by a factor of 0.853. The fibers are thus expected to have transmission bands of same width, with positions shifted by a factor of Λ_A/Λ_B.

Transmission spectra were measured with a white light Halogen-Tungsten lamp of the fibers coiled with a single turn of varying diameter. In all measurements, the fibers are bent with the coil plane parallel to the axis of the Ge-doped rods, and with the small Ge-doped rods on the outside of the bend with respect to coil center. A pick-up fiber with core diameter of 25 μm and NA = 0.6 is used to collect the core light, thereby spatially filtering out the cladding light. The spectral content is analyzed with an Optical Spectrum Analyzer (OSA), and the results are shown in Fig. 3(a), for fiber A, and 3(b), for fiber B.
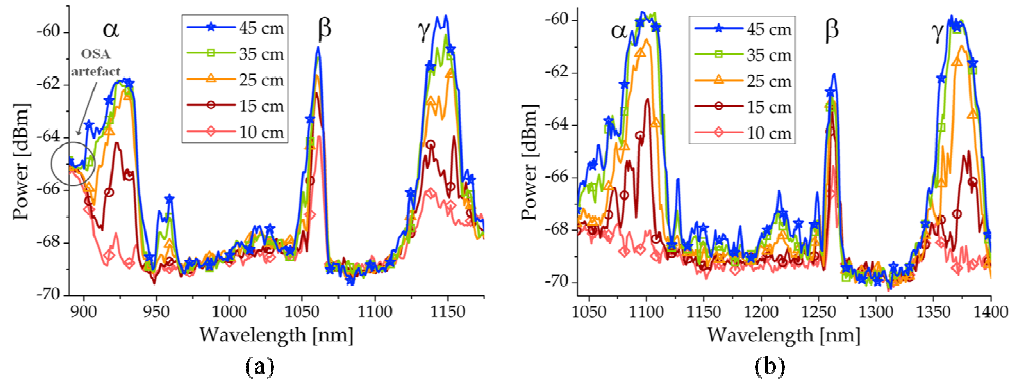

Fig. 3. White light transmission spectra of fiber A, (a), and fiber B, (b), coiled with a single turn of different diameter. The power increase for wavelengths shorter than ~900 nm in (a) is an artefact of the optical spectrum analyzer and not a guiding property of the fiber. The same three transmission bands are observed in both fibers; transmission band α, β, and γ.
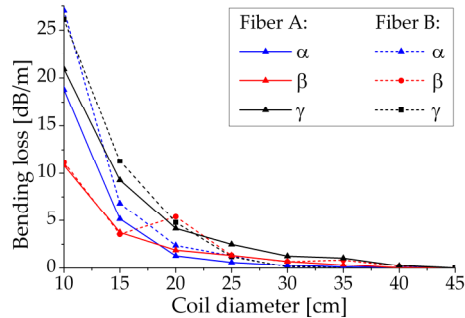

Fig. 4. Bending loss in transmission band α, β, and γ as a function of coil diameter. The largest coil diameter is used as a reference of zero bending loss.

Spectral stop bands are clearly observed in Fig. 3, while an increased power is measured in three spectral ranges corresponding to the transmission bands. In Fig. 3(a) and 3(b) the same three transmission bands are observed, named for future reference as α, β, and γ. The suppression in the stop bands depends to some degree on the measurement circumstances. The pick-up fiber will unavoidable collect both core and some cladding light. The collected cladding light increases the power level in the stop bands, thus reducing the measured suppression. If the pick-up fiber is offset with respect to the core center or if the input is not launched directly in the core, a higher amount of cladding light will be collected. A power increase is observed for wavelengths lower than ~900 nm in Fig. 3(a). This increase is not a guiding property of the fiber, but an artefact of the OSA.

Figure 4 shows the bending loss in the transmission bands as a function of coil diameter. The fibers are quite bending resistant for coil diameters down to ~30 cm, demonstrating the possibility to use the fibers in compact amplifier setups. In transmission band β of fiber B a sudden increase in the bendloss is observed for a coil diameter of 20 cm. The same tendency

is not observed in transmission band α or γ. The increase is probably caused by coupling to a resonant cladding mode at this coil diameter. For coil diameters of 10 cm and 15 cm, transmission band β experiences the lowest bending loss.

The difference in bending loss of α, β, and γ for small coil diameters is caused by the behaviour of the cladding modes. The different sizes of Ge-doped rods cause two sets of cladding modes - one set due to the large Ge-doped rods, and one set due to small Ge-doped rods. Fiber bending has the same effect as a tilting of the refractive index profile [6]. Since the large Ge-doped rods are only present on the inside of the bend with respect to coil center, a decrease of the effective refractive index of the corresponding cladding modes occurs with decreasing coil diameter. The small Ge-doped rods are only present on the outside of the bend, thus the effective refractive index of the corresponding cladding modes will increase. The result is that transmission bands having the blue edge determined by the small Ge-doped rods and the red edge determined by the large Ge-doped rods will narrow spectrally with decreasing coil diameters. Such transmission bands correspond to the overlap of two identical ordered bandgaps, one caused by the large Ge-doped rods and one caused by the small Ge-doped rods. On the contrary, transmission bands having the blue edge determined by the large Ge-doped rods and the red edge determined by the small Ge-doped rods broadens spectrally with decreasing coil diameter. Such transmission bands result from the overlap of different ordered bandgaps.
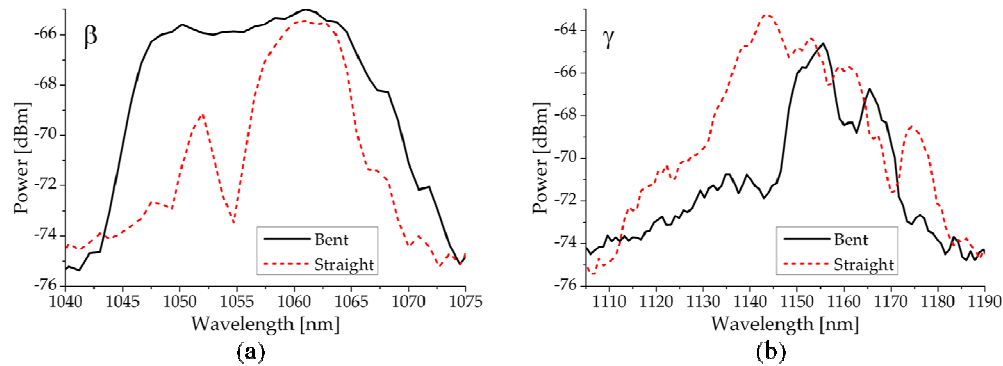

Fig. 5. White light transmission spectra of fiber A. In (a) transmission band β is seen, in (b) transmission band γ. In the bent case the fiber is coiled with three turns to a coil diameter of 20 cm, such that the entire fiber is bent.

Transmission bands α and γ result from overlaps of identical ordered bandgaps, thus they spectrally narrow with decreasing coil diameter. On the contrary, transmission band β results from overlaps of two different ordered bandgaps, and should broaden with decreasing coil diameter. When the measurements shown in Fig. 3 were performed, the PCFs were coiled with a single turn, and straight sections were present at both ends of the fiber. To observe the broadening of transmission bands, the entire fiber needs to be coiled in the measurement. White light transmission measurements were performed for fiber A, with the entire fiber coiled. The results for transmission band β and γ are shown in Fig. 5.

The bending properties demonstrated in Fig. 5(a) are unique for the asymmetric hybrid fiber. Spectral broadening of transmission bands with decreasing coil diameters is not observed in symmetric hybrid fibers, PBG fibers or any other fibers. This novel bending property adds a new dimension to the asymmetric hybrid fiber, since the fiber can be coiled very tightly without losing the guiding properties in the broadening transmission bands. Numerical investigations have verified the unique bending properties and large core confinement of the mode in transmission band β for coil diameters as low as 10 cm [7].

3.2 Single-mode properties

Different methods for quantifying the SM properties of the PCFs exist. One is the spatially and spectrally resolved imaging of the mode content in the fiber, or simply the S^2 method [8]. S^2 is based on the group delay difference of the fiber modes which give rise to spectral interference. The method thus requires significant bandwidth, to measure the HOM content, and is not suitable for single wavelength investigation in narrow bandgaps.

Another approach is the M^2 method, but it has been shown, that unity M^2 values not necessarily indicate SM propagation [9]. The M^2 value depends on the actual mode profile [10], and in the considered fiber the mode has a slightly hexagonal shape, due to the lattice structure of the photonic crystal cladding, and hence M^2 will be larger than unity.

The SM performance of the asymmetric hybrid PCFs is instead investigated qualitatively by considering the output beam profile of the fiber with a near-field camera while translating the input beam in the transverse direction of the fiber. If Higher-Order Modes (HOMs) are present the beam profile will depend on launching conditions, but if no HOMs are present, the beam profile will only be attenuated.
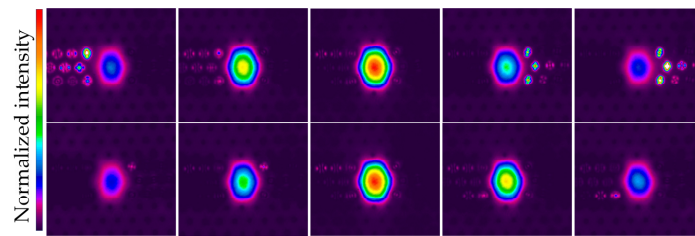

Fig. 6. Near-field images of the output of fiber B at 1100 nm. The input is translated along the Ge-doped rods (top row) and orthogonally to the Ge-doped rods (bottom row). The center images show the input launched directly in the core. Only the fundamental mode is observed.

Figure 6 shows a series of near-field images of fiber B (2 m) coiled to 60 cm diameter, single turn, when an 1100 nm wavelength input beam with spot size 30 μm is translated in the transverse direction of the core. The beam profile does not exhibit any modal changes, and is only attenuated. This indicates no or very little HOM content in the core. The fiber is thus SM operated for coil diameters as large as 60 cm.

4. Improved properties of the 3-row design

4.1 Spectral and spatial filter

The hybrid asymmetric PCF amplifier design was first presented in [11], but with only one row of Ge-doped rods. Compared to the 1-row design the 3-row design has some clear advantages. An essential advantage is enhanced suppression in the stop bands, improving the gain-shaping properties. The improvement can be quantified numerically by the overlap integral of the fundamental mode with the doped core region, Γ [12]. Γ is calculated with a full-vector modal solver based on the finite element method [13], which is used for all numerical computations presented in this paper. The results are seen in Fig. 7(a). In the calculations, fibers of the 1- and 3-row design have been considered, both having $\Lambda_{num} = 10$ μm, $d_{air} = 0.15\Lambda_{num}$, large Ge-doped rod diameter of $0.71\Lambda_{num}$, and a small Ge-doped rod diameter reduced by a factor of 0.83 with respect to the large Ge-doped rod diameter. For large values of Γ the mode is well-confined in the core, and the three transmission bands, α, β, and γ, are observed in the spectrum.

In Fig. 7(b) a white light transmission spectrum of fiber B is compared with a white light transmission spectrum of a 1-row fiber. The 1-row fiber is 2 m long, having $\Lambda_{1\text{-row}} = 10$ μm and $d_{air} = 0.14\Lambda_{1\text{-row}}$. In this fiber the large Ge-doped rods have a diameter of 0.71Λ, while the small Ge-doped rods are reduced by a factor of 0.86. Both fibers are coiled with a single

turn of diameter 45 cm, having the small Ge-doped rods outwards with respect to coil center. The differences in transmission band β in the 1- and 3-row design are due to size-differences in the Ge-doped rods of the two fibers. Furthermore, the 1-row design is Yb-doped resulting in absorption near $\lambda/\Lambda = 0.100$, which causes the output power decrease in this region. The differences between the numerical and experimental results in Fig. 7 are due to the different dimensions of the Ge-doped rods, and the actual index profile of the Ge-doped rods is hard to simulate, since it can change during fabrication of the fibers.
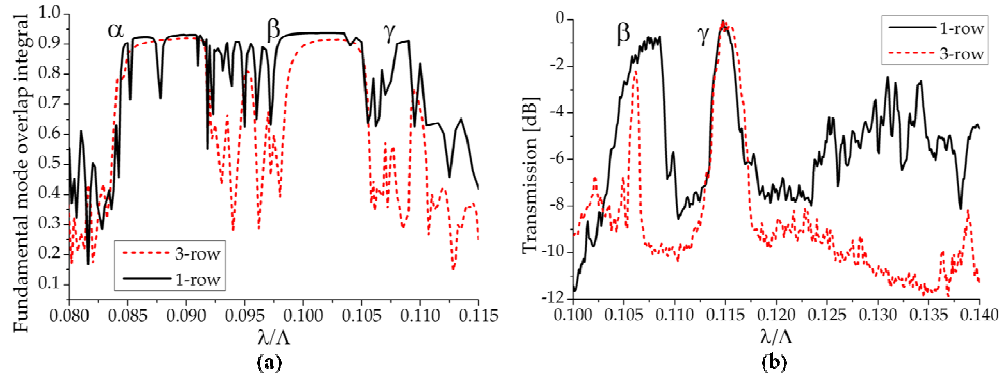

Fig. 7. (a) Calculated overlap integral of the fundamental mode with doped core region for the 1- and 3-row design, simulated with a coil of diameter 40 cm. (b) White light transmission spectra of the 1- and 3-row design scaled according to maximum power value. The fibers are coiled with a single turn of diameter 45 cm. The wavelength, λ, is normalized to the pitch size, Λ.

In Fig. 7(a) a large decrease in the overlap integral values obtained for the 3-row design, with respect to the values obtained for the 1-row design, is observed in the stop bands for the entire spectral range. Experimentally, the enhanced suppression in the stop bands is especially clear in the region $\lambda/\Lambda = 0.125\text{-}0.14$, as shown in Fig. 7(b). The improved suppression in the 3-row design is a result of the increasing resemblance with a full PBG fiber. If only one row of Ge-doped rods is present the formation of broadband cladding modes is limited with respect to a PBG fiber, since coupling between fewer Ge-doped rods occur [14]. This effect is reduced by introducing a larger number of Ge-doped rods in the 3-row design, and a better spectral filter is obtained.

The spatial filtering properties of the fiber are also influenced by the number of rows of Ge-doped rods. In Fig. 8 the magnetic field modulus distribution of the LP_{11}-like mode with zero along the axis of the Ge-doped rods is seen in the 1- and 3-row design in the stop band at $\lambda/\Lambda = 0.113$, Fig. 8(a) and 8(b) respectively. The modes are calculated with the modal solver. The 1-row design has $\Gamma = 0.71$, for the 3-row design the value is reduced relatively with ~34% to $\Gamma = 0.47$. Γ depends on the spatial distribution of the mode in the core with respect to the position of the Ge-doped rods. In the 1-row design the mode overlap with the Ge-doped rods is low, thus filtering of the mode is hard to achieve. In the 3-row design the overlap of the mode with the Ge-doped rods increases significantly, and the mode is filtered more effectively.

For the LP_{11}-like mode with zero along the axis orthogonal to the axis of the Ge-doped rods the impact is not as significant. The spatial distribution ensures a high overlap with the Ge-doped rods both in the 1- and 3-row design and in both designs Γ is less than 0.3.

The extra rows of Ge-doped rods in the 3-row design therefore improve both the spectral and spatial filtering.
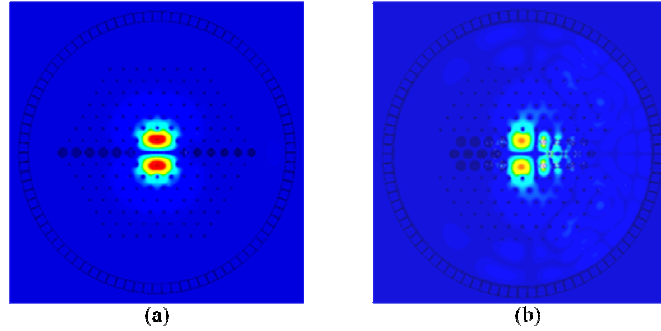
Fig. 8. Magnetic field modulus distribution of the LP_{11}-like mode in (a) the 1-row design and (b) the 3-row design at $\lambda/\Lambda = 0.113$. The mode distribution is calculated with a full-vector modal solver based on the finite element method [13]. For (a) the overlap integral of the fundamental mode with the doped core region is 0.71, for (b) the value is 0.47.

4.2 Polarization properties

The two-fold symmetry of the hybrid asymmetric PCF gives both form- and stress birefringence, whereas the latter gives the highest contribution. Stress birefringence is caused by the Ge-doped rods having a different thermal expansion coefficient than silica. The 3-row design is thus expected to have more birefringence than the 1-row design.

Two different birefringence values can be deduced, the modal birefringence and the group birefringence. The modal birefringence is the most important parameter for a polarization maintaining fiber, since it describes the fibers ability to maintain linear polarization [14]. The modal birefringence is given by:

$$B_m(\lambda) = n_x(\lambda) - n_y(\lambda) \tag{1}$$

where $B_m(\lambda)$ is the modal birefringence, $n_x(\lambda)$ and $n_y(\lambda)$ are the phase refractive indices for the two orthogonally polarized modes, and λ is the wavelength. $n_x(\lambda)$ and $n_y(\lambda)$ are found with the modal solver, and the modal birefringence is calculated according to Eq. (1) for the same fibers as considered in Fig. 7(a). The results of the 1- and 3-row design are compared in Fig. 9(a). The flat regions correspond to the positions of the transmission bands, and only these are of interest. $B_m(\lambda)$ of the 1-row design is $\sim 3 \cdot 10^{-5}$, while for the 3-row design the value is $\sim 8 \cdot 10^{-5}$, a relative increase of 2.7 in the 3-row design.
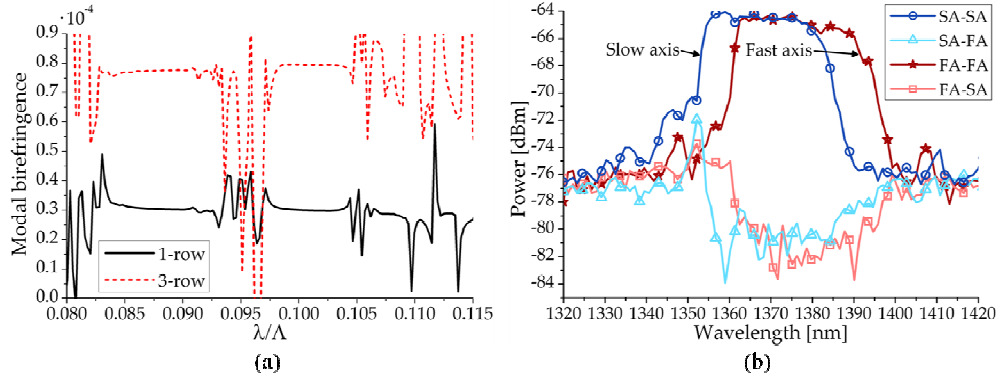

Fig. 9. (a) Calculated modal birefringence in the 1- and 3-row design. The modal birefringence is increased with a factor of ~2.7 in the 3-row design. (b) Polarization properties of transmission band γ.

The polarizing properties of the fiber B are investigated with a crossed polarizer setup. Unpolarized white light from a Halogen-Tungsten lamp is launched through a polarizer along the slow axis/fast axis (SA/FA) and is collected in the pick-up fiber after a second polarizer aligned along the SA/FA or FA/SA. The results of transmission band γ are seen in Fig. 9(b). The SA is clearly blue shifted with respect to the FA as expected, and a suppression of ~18 dB is observed for both axes when the output polarizer is in the SA/FA and FA/SA position. For the configurations SA-FA and FA-SA the suppression in the transmission band is larger than in the stop bands. This behaviour reflects cladding light being collected in the pick-up fiber. In the transmission band the mode is confined in the core and do not couple to any cladding modes. Thus the amount of cladding light is reduced. In the stop bands the core mode filters by coupling to cladding modes resulting in the amount of cladding light increases. The core mode do not contribute to the amount of cladding light being collected inside the transmission bands, so when the polarizers are in the SA-FA/FA-SA configuration the core mode is blocked and the power level decreases from the level in the stop bands.

5. Transmission band for amplification

The improved spectral and spatial filtering properties and the increased birefringence of the 3-row design with respect to the 1-row one, make the former a more advantageous candidate for the fiber amplifier. The transmission band suitable for amplification has to satisfy some specific demands. The most important requirement is efficient suppression of ASE below the signal wavelength. If amplification near 1178 nm is desired, ASE should be suppressed in the spectral range ~1020 nm - 1175 nm. This corresponds to a suppression bandwidth of 14.1% relative to the center wavelength of this range. At wavelengths shorter than the blue edge of transmission band α a suppression bandwidth of 17.8% is observed. Therefore transmission band α fulfils the requirement.

Adjacent transmission bands behave very differently with respect to bending properties; one type narrows and the other broadens with decreasing coil diameter. The signal wavelength should be positioned close to the blue edge of the transmission band of interest. In transmission bands that broaden with decreasing coil diameter, the blue edge moves towards shorter wavelengths with tighter bending, and new spectral components can enter the transmission band, which might cause ASE at unwanted wavelengths. On the contrary, in transmission bands that narrow with decreasing coil diameter, the blue edge red shifts with bending, and the signal wavelength can fall outside of the transmission band, which can reduce the amplification. However, both properties can also be used to tailor the transmission band, if it is either too narrow or too wide. To utilize the broadening effect the entire fiber needs to be coiled, whereas the narrowing effect does not require the fiber entirely bent. Therefore, the broadening effect can be harder to control and thereby to utilize, making the narrowing transmission band preferable for amplification. Transmission band α narrows with bending, for the fiber oriented with the small Ge-doped rods outwards, and thus fulfils also this preference.

6. Ytterbium-doped fibers

One Yb-doped PCF of the 3-row design, named fiber C, is considered in this section. The fiber has $\Lambda_C = 12.9$ μm and $d_{air,C} = 0.16\Lambda_C$, resulting in a core diameter of ~45 μm. The large Ge-doped rods have a diameter of 0.71Λ, while the small Ge-doped rods are down-scaled by a factor of 0.835 with respect to the large ones. The blue edge of transmission band α is determined by the small Ge-doped rods, so the slight decrease in the ratio between the diameters of the small and large Ge-doped rods results in a spectral broadening of transmission band α in fiber C, with respect to fiber A and B. The blue edge of transmission band α in fiber B is situated near 1070 nm, thus the blue edge of transmission band α in fiber C is expected to be positioned near $\Lambda_C/\Lambda_B \cdot 0.835/0.853 \cdot 1075$ nm = 1131 nm. For

amplification at longer wavelengths the pitch size must be increased, and the gain shaping properties of fiber C are also illustrative of the function of the fiber at longer wavelengths.

The SM performance of fiber C is investigated with the method described in Sec. 3.2. Figure 10 shows a series of near-field images of fiber C (2 m) coiled to 40 cm diameter, single turn, when an 1178 nm wavelength input beam with spot size 30 μm is translated in the transverse direction of the core. The beam profile does not exhibit any modal changes, and is only attenuated. This indicates no or very little HOM content also in the Yb-doped PCF.

The impact of gain shaping in the considered fiber is investigated by multiplying the suppression in the stop band, observed in the white light transmission measurements, with the gain spectrum. If the fraction of excited ions is averaged over the fiber length, the gain spectrum, $G(\lambda)$, is given by [15]:

$$G(\lambda) = 4.343\Gamma_s L N_0 \left[\left(\sigma_e(\lambda) + \sigma_a(\lambda) \right) n_2 - \sigma_a(\lambda) \right] \qquad (2)$$

Where Γ_s is the signal mode overlap with the doped core region, L is the fiber length, N_0 is the Yb concentration, $\sigma_e(\lambda)$ and $\sigma_a(\lambda)$ are the emission and absorption cross-section spectra respectively, and n_2 is the fraction of Yb in the excited state averaged over the fiber length. The gain spectra obtained for different fractions of Yb-ions in the excited state, considering a typical dopant concentration of $N_0 = 0.38 \cdot 10^{20}$ cm^{-3} and $\Gamma_s = 1$, are shown in Fig. 11(a).
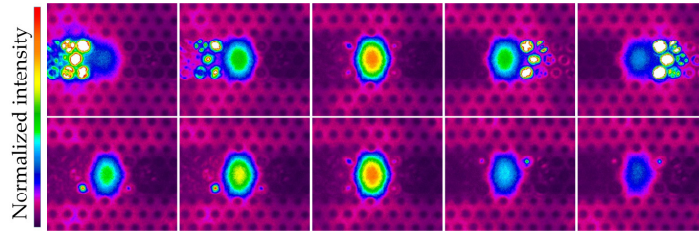

Fig. 10. Near-field images of the output of fiber C at 1178 nm. The input is translated along the Ge-doped rods (top row) and orthogonally to the Ge-doped rods (bottom row). The center images show the input launched directly in the core. Only the fundamental mode is observed.
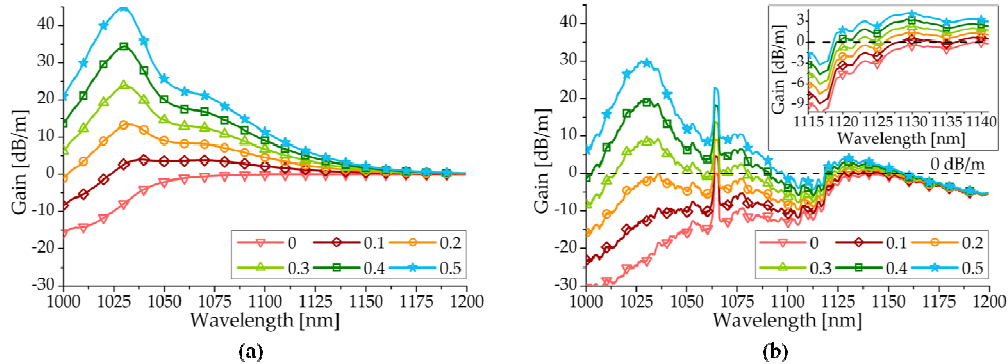

Fig. 11. (a) Gain spectra of an Yb^{3+}-doped aluminosilicate fiber for different fractions of excited Ytterbium-ions, n_2, given in the legend. The gain is calculated according to Eq. (2) for an Ytterbium concentration of $N_0 = 0.38 \cdot 10^{20}$ cm^{-3}, and for a signal mode overlap with the doped core region of $\Gamma_s = 1$. (b) Gain shaping in fiber C of the spectra shown in (a). For $n_2 \leq$ 0.2 the maximum gain is obtained at 1130 nm. The peak observed at 1064 nm is due to the light source used in the transmission measurement in fiber C, and will therefore not influence the gain shaping in the amplifier.

To illustrate the gain shaping in fiber C, a transmission measurement was performed in 1 m of fiber in a straight configuration with a SuperK Compact (NKT Photonics)

supercontinuum white light laser. A reference measurement was subtracted the transmission measurements, the 1064 nm peak is the supercontinuum pump. This transmission spectrum can be used to numerically demonstrate the properties of the Yb-doped gain shaping PCF, since the gain spectrum in fiber C is modulated with respect to the one given in Eq. (2).

Gain shaping in fiber C is calculated and seen in Fig. 11(b). The insert in the right upper corner shows the gain curves at the blue edge of transmission band α, which is positioned near 1130 nm. A shift of the gain maximum in fiber C is clearly observed comparing Fig. 11(a) and Fig. 11(b) for $n_2 \leq 0.2$. In this region the maximum gain is obtained at 1130 nm, with a value of 1.4 dB/m for $n_2 = 0.2$. However for n_2 exceeding 0.2 the maximum gain shifts from 1130 nm to 1030 nm. Since a white light transmission spectrum is used as a reference of the suppression, this depends on the amount of cladding light also being collected in the pick-up fiber. The suppression is thus larger than observed, resulting in the maximum gain being positioned at 1130 nm for even higher fractions of Yb-ions in the excited state.

7. Conclusions

In this work, a novel design of an Yb-doped fiber amplifier suitable for amplification in the long wavelength region of the Yb emission spectrum, above 1100 nm, was studied. Two guiding mechanisms of the photonic crystal are combined in a hybrid fiber design; index- and bandgap guiding. The index guiding enables a very LMA core design, without compromising SM behavior. Bandgap guiding gives rise to gain shaping, such that the maximum of the Yb gain spectrum can be shifted towards longer wavelengths. The proposed hybrid PCF has three rows of high-index inclusions on each side of the core, a 3-row design. The high-index rods on one side of the core are reduced in size with respect to the rods on the other, resulting in an asymmetric design. The PCF was compared to a prior design having one row of high-index inclusions. The 3-row PCF has a larger suppression of ASE, improved gain shaping properties, and the modal birefringence is increased with a factor of ~2.7. The PCF can be coiled to diameters of ~30 cm without losing confinement of the core mode, and can therefore be used in compact amplifier setups. The asymmetry of the PCF causes bending properties not observed in any other PBG fibers. In particular, broadening of certain transmission bands occur for decreasing coil diameters. SM behaviour at 1178 nm was demonstrated in a PCF with core diameter of ~45 μm, and the build-in gain shaping was demonstrated by a red-shifting of the maximum gain from 1030 nm to 1130 nm.

Acknowledgment